

Trust-Region Neural Moving Horizon Estimation for Robots

Bingheng Wang, Xuyang Chen, and Lin Zhao

Abstract— Accurate disturbance estimation is essential for safe robot operations. The recently proposed neural moving horizon estimation (NeuroMHE), which uses a portable neural network to model the MHE’s weightings, shows promise in this context. Currently, NeuroMHE is trained through gradient descent, with its gradient computed recursively using a Kalman filter. This paper proposes a trust-region policy optimization method for training NeuroMHE. We achieve this by providing the second-order derivatives of MHE, referred to as the MHE Hessian. Remarkably, we establish that much of computation already used to obtain the gradient, especially the Kalman filter, can be efficiently reused to compute the MHE Hessian. This offers linear computational complexity relative to the MHE horizon. Through validation with an open-source real quadrotor flight dataset, our approach demonstrates data-efficient training (< 5 min) and outperforms a state-of-the-art neural estimator by up to 68.1% in force estimation accuracy, utilizing only 1.4% of its network parameters. Furthermore, our method showcases enhanced robustness to network initialization compared to the gradient descent counterpart.

SUPPLEMENTARY MATERIAL

We released our source code at <https://github.com/BinghengNUS/TR-NeuroMHE>

I. INTRODUCTION

Disturbances are widespread in robot operations across tasks, arising from various sources including system uncertainties [1], aerodynamic influences [2], ground friction forces [3], and hydrodynamic disturbances [4]. Addressing these disturbances is vital in robotic control to prevent significant performance degradation [5], [6]. However, the intricate nature of these disturbances renders prediction using a portable model infeasible. Therefore, online precise disturbance estimation that adapts to environments is crucial for safe and effective robot operations.

Early works in disturbance estimation mainly utilize either model-based solutions or model-free learning techniques. While model-based estimators are data-efficient, they often struggle to capture general cases, as the models used are typically limited to specific slowly-varying disturbances [7]–[9]. Another challenge lies in their heavy reliance on manually tuning numerous parameters [10], [11], which demands significant experimental efforts and expert knowledge. In contrast, model-free approaches using neural networks (NN) can achieve high performance across various disturbance scenarios with minimal expert knowledge. Examples include estimating system uncertainties for robotic joints [12] and

These authors are with the Department of Electrical and Computer Engineering, National University of Singapore, 4 Engineering Drive 3, 117583 Singapore, Singapore {wangbingheng, chenxuyang}@u.nus.edu, elezhli@nus.edu.sg

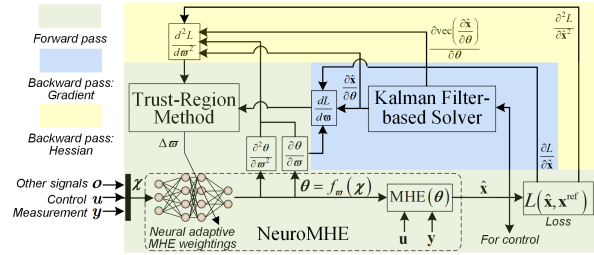


Fig. 1: Learning pipelines of the trust-region NeuroMHE. Currently, NeuroMHE is trained via gradient descent with its gradient computed recursively using a Kalman filter. This paper enhances NeuroMHE training with the second-order trust-region method. Interestingly, we show that the MHE Hessian trajectory can be obtained recursively using the same Kalman filter.

complex aerodynamic effects for aerial robots [13], [14]. In practice, these NN-based estimators typically use large network models for training, along with substantial disturbance data and complicated learning curricula.

To leverage advantages from both model-free and model-based methods, we recently proposed the neural moving horizon estimation (NeuroMHE) [15]. This algorithm fuses a portable neural network into an MHE to realize accurate estimation and fast online adaptation (See the dashed block in Fig. 1). MHE, a control-theoretic optimal state estimator, addresses dynamic nonlinear optimization online in a receding horizon manner. It has consistently demonstrated superior performance in disturbance estimation for both ground [16] and aerial [17], [18] robots. Nevertheless, the parameter tuning remains a persistent challenge for vanilla MHE, especially when dealing with dynamic and nonlinear parameters in practical applications [19]. In contrast, NeuroMHE tackles this challenge by modeling its parameters using the neural network trained through gradient descent. The gradient includes the derivative of MHE’s optimal solution trajectory with respect to (w.r.t) the parameters, computed recursively using a Kalman filter. This approach achieves linear computational complexity relative to the MHE horizon, substantially improving training efficiency compared to state-of-the-art auto-tuning MHE methods [20], [21].

In this paper, we enhance NeuroMHE training by providing second-order derivative information of MHE (i.e., the MHE Hessian). This allows us to employ the trust-region method, a second-order optimization technique, for training NeuroMHE. Unlike gradient descent, the trust-region method offers adaptive step-size updates, faster convergence, and improved robustness to initialization. It has shown efficacy across machine learning and robotics, including policy optimization [22] and, more recently, synergizing optimal control with inverse reinforcement learning [23]. Our work

contributes to this interdisciplinary collection by introducing another general second-order policy optimization method for estimation. Fig. 1 outlines the learning pipelines of the trust-region NeuroMHE. Two key ingredients of our algorithm are the gradient and Hessian trajectories of the MHE’s optimal solutions w.r.t the parameters in the backward passes. By differentiating the Karush-Kuhn-Tucker (KKT) conditions of the MHE optimization problem in the forward pass, we can efficiently obtain the MHE gradient trajectory using a Kalman filter, as validated in [15]. Interestingly, we demonstrate that the same Kalman filter can be reused to compute the MHE Hessian trajectory with only minor modifications to its inputs, which are acquired through double differentiation of the KKT conditions. This preserves the linear computational complexity w.r.t the MHE horizon, further improving the training efficiency.

We evaluate the effectiveness of the proposed trust-region NeuroMHE by comparing it with a state-of-the-art method NeuroBEM [13] for estimating complex aerodynamic disturbances on a quadrotor, utilizing NeuroBEM’s real flight dataset. We show that compared with the NeuroBEM, our method 1) enjoys highly efficient training (< 5 min); 2) uses only 1.4% of the network parameters; and 3) reduces the overall force estimation error by up to 68.1%. Further comparisons with the gradient descent counterpart demonstrate that, although computing the MHE Hessian trajectory naturally takes longer than the gradient trajectory, our method significantly reduces both the total training episodes and the overall training time. Additionally, our approach exhibits lower sensitivity to the initialization of the neural network. In summary, our contributions are threefold:

- 1) We propose a trust-region policy optimization method for training the recently developed NeuroMHE.
- 2) We demonstrate that much of computation used to obtain the MHE gradient trajectory, particularly the Kalman filter, can be efficiently reused for computing the MHE Hessian trajectory in a recursive manner.
- 3) We validate the effectiveness of our approach using a real flight dataset, showing highly efficient training and superior performance compared to the state-of-the-art method in aerodynamic force estimation accuracy.

The rest of this paper is organized as follows. Section II briefly reviews the formulation of NeuroMHE. In Section III, we detail the process of reusing the Kalman filter to compute the MHE Hessian. Section IV develops the proposed trust-region NeuroMHE training method. Simulation results on the real dataset are reported in Section V. We conclude this paper and discuss our future work in Section VI.

II. PRELIMINARY OF NEUROMHE

A. Moving Horizon Estimation

MHE is a model-based optimal state estimator. Without loss of generality, we assume that the robotic dynamics model used in MHE takes the following form:

$$\dot{\mathbf{x}} = \mathbf{f}(\mathbf{x}, \mathbf{u}, \mathbf{w}), \quad \mathbf{y} = \mathbf{h}(\mathbf{x}) + \boldsymbol{\nu}, \quad (1)$$

where $\mathbf{x} \in \mathbb{R}^n$ is the system state, $\mathbf{u} \in \mathbb{R}^m$ is the control input, the system model \mathbf{f} is subject to the process noise $\boldsymbol{\nu} \in \mathbb{R}^w$, \mathbf{h} is the measurement function, and $\mathbf{y} \in \mathbb{R}^l$ denotes the measurement subject to the noise $\boldsymbol{\nu} \in \mathbb{R}^l$. Given the most recent measurements $\mathbf{y} = \{\mathbf{y}_k\}_{k=t-N}^t$ and control inputs $\mathbf{u} = \{\mathbf{u}_k\}_{k=t-N}^{t-1}$ collected in a moving data window of horizon N , the MHE estimator optimizes over $\mathbf{x} = \{\mathbf{x}_k\}_{k=t-N}^t$ and $\mathbf{w} = \{\mathbf{w}_k\}_{k=t-N}^{t-1}$ at each time step $t \geq N$ by solving the following optimization problem online.

$$\min_{\mathbf{x}, \mathbf{w}} J = \underbrace{\frac{1}{2} \|\mathbf{x}_{t-N} - \hat{\mathbf{x}}_{t-N}\|_{\mathbf{P}}^2}_{\text{arrival cost}} + \underbrace{\frac{1}{2} \sum_{k=t-N}^t \|\mathbf{y}_k - \mathbf{h}(\mathbf{x}_k)\|_{\mathbf{R}_k}^2 + \frac{1}{2} \sum_{k=t-N}^{t-1} \|\mathbf{w}_k\|_{\mathbf{Q}_k}^2}_{\text{running cost}} \quad (2a)$$

$$\text{s.t. } \mathbf{x}_{k+1} = \mathbf{f}(\mathbf{x}_k, \mathbf{u}_k, \mathbf{w}_k, \Delta t), \quad (2b)$$

where $\mathbf{P} \in \mathbb{R}^{n \times n}$, $\mathbf{R}_k \in \mathbb{R}^{l \times l}$, and $\mathbf{Q}_k \in \mathbb{R}^{w \times w}$ are the positive-definite weighting matrices, \mathbf{f} is the discrete-time model of \mathbf{f} with the step-size of Δt for predicting the state, and $\hat{\mathbf{x}}_{t-N}$ is the filter priori which is chosen as the MHE’s optimal estimate $\hat{\mathbf{x}}_{t-N|t-1}$ of \mathbf{x}_{t-N} obtained at $t-1$ [24]. We denote by $\hat{\mathbf{x}} = \{\hat{\mathbf{x}}_{k|t}\}_{k=t-N}^t$ and $\hat{\mathbf{w}} = \{\hat{\mathbf{w}}_{k|t}\}_{k=t-N}^{t-1}$ the MHE’s optimal solutions to Problem (2) at time step t .

B. Formulation of NeuroMHE

The weighting matrices in the cost function (2a) are the tuning parameters, which determine the MHE performance. For ease of presentation, we represent them in a vector $\boldsymbol{\theta} = [vec(\mathbf{P}), \{vec(\mathbf{R}_k)\}_{k=t-N}^t, \{vec(\mathbf{Q}_k)\}_{k=t-N}^{t-1}] \in \mathbb{R}^p$ where $vec(\cdot)$ denotes the vectorization of a given matrix. Tuning $\boldsymbol{\theta}$ typically necessitates a priori knowledge of the covariances of the noises entering robotic systems. Identifying these noise covariances is difficult in practice due to their large number and strong coupling. It becomes even more demanding when these values exhibit dynamic behavior.

NeuroMHE tackles the above challenge by modeling $\boldsymbol{\theta}$ with a portable neural network:

$$\boldsymbol{\theta} = \mathbf{f}_{\boldsymbol{\varpi}}(\boldsymbol{\chi}). \quad (3)$$

The neural network can accept various signals as its inputs $\boldsymbol{\chi}$, including measurements \mathbf{y} , controls \mathbf{u} , and other external signals \mathbf{o} , depending on specific applications. Its parameters $\boldsymbol{\varpi}$ are trained using powerful machine learning techniques. Here, $\boldsymbol{\varpi}$ represents the tuning parameters for NeuroMHE, and we parameterize Problem (2) as NeuroMHE($\boldsymbol{\varpi}$), with the MHE’s solution denoted as $\hat{\mathbf{x}}(\boldsymbol{\varpi})$. Then, the training can be interpreted as the following optimization problem:

$$\min_{\boldsymbol{\varpi}} L(\hat{\mathbf{x}}(\boldsymbol{\varpi})) \quad (4a)$$

$$\text{s.t. } \hat{\mathbf{x}}(\boldsymbol{\varpi}) \text{ generated by NeuroMHE}(\boldsymbol{\varpi}). \quad (4b)$$

Here $L(\hat{\mathbf{x}}(\boldsymbol{\varpi}))$, a loss function assessing NeuroMHE’s performance, can be built upon estimation errors when ground

truth state data is accessible. Alternatively, it can be tailored to penalize tracking errors in applications involving robust trajectory tracking control.

III. ANALYTICAL HESSIAN TRAJECTORY

Our previous work [15] solved Problem (4) using gradient descent, with the gradient computed recursively through a Kalman filter. In this section, our objective is to efficiently reuse the same Kalman filter and much of computation initially employed to obtain the gradient. We intend to apply these resources in computing the MHE Hessian for training NeuroMHE with second-order optimization techniques.

A. Kalman Filter-based Gradient Solver

The gradient of $L(\hat{\mathbf{x}}(\boldsymbol{\varpi}))$ w.r.t $\boldsymbol{\varpi}$ can be calculated using the chain rule:

$$\nabla_{\boldsymbol{\varpi}} L(\hat{\mathbf{x}}(\boldsymbol{\varpi})) = \nabla_{\hat{\mathbf{x}}} L(\hat{\mathbf{x}}) \nabla_{\boldsymbol{\theta}} \hat{\mathbf{x}}(\boldsymbol{\theta}) \nabla_{\boldsymbol{\varpi}} \boldsymbol{\theta}(\boldsymbol{\varpi}). \quad (5)$$

The gradients $\nabla_{\hat{\mathbf{x}}} L$ and $\nabla_{\boldsymbol{\varpi}} \boldsymbol{\theta}$ are straightforward to obtain as both $L(\hat{\mathbf{x}})$ and $\boldsymbol{\theta}(\boldsymbol{\varpi})$ are explicit functions. The main challenge lies in the computation of $\nabla_{\boldsymbol{\theta}} \hat{\mathbf{x}}$. Recall that $\hat{\mathbf{x}}(\boldsymbol{\theta})$ is the MHE's solution, with its dependence on $\boldsymbol{\theta}$ implicitly defined via the necessary optimality conditions. This implicit definition enables us to compute $\nabla_{\boldsymbol{\theta}} \hat{\mathbf{x}}$ by differentiating through the KKT conditions of Problem (2). To proceed, we associate the equality constraints (2b) with the dual variables $\boldsymbol{\lambda} = \{\boldsymbol{\lambda}_k\}_{k=t-N}^{t-1}$ and denote $\boldsymbol{\lambda}^* \in \mathbb{R}^n$ as their optimal values. The corresponding Lagrangian can be written as

$$\mathcal{L} = J + \sum_{k=t-N}^{t-1} \boldsymbol{\lambda}_k^T (\mathbf{x}_{k+1} - \mathbf{f}(\mathbf{x}_k, \mathbf{u}_k, \mathbf{w}_k, \Delta t)). \quad (6)$$

Then the KKT conditions of Problem (2) at $\hat{\mathbf{x}}$, $\hat{\mathbf{w}}$, and $\boldsymbol{\lambda}^*$ are given by

$$\nabla_{\hat{\mathbf{x}}_{t-N|t}} \mathcal{L}(\hat{\mathbf{x}}_{t-N|t}, \hat{\mathbf{x}}_{t-N}, \hat{\mathbf{w}}_{t-N|t}, \boldsymbol{\lambda}_{t-N}^*, \boldsymbol{\theta}) = \mathbf{0}, \quad (7a)$$

$$\nabla_{\hat{\mathbf{x}}_{k|t}} \mathcal{L}(\hat{\mathbf{x}}_{k|t}, \hat{\mathbf{w}}_{k|t}, \boldsymbol{\lambda}_k^*, \boldsymbol{\lambda}_{k-1}^*, \boldsymbol{\theta}) = \mathbf{0}, \quad (7b)$$

$$\nabla_{\hat{\mathbf{w}}_{k|t}} \mathcal{L}(\hat{\mathbf{x}}_{k|t}, \hat{\mathbf{w}}_{k|t}, \boldsymbol{\lambda}_k^*, \boldsymbol{\theta}) = \mathbf{0}, \quad (7c)$$

$$\nabla_{\boldsymbol{\lambda}_k^*} \mathcal{L} = \hat{\mathbf{x}}_{k+1|t} - \mathbf{f}(\hat{\mathbf{x}}_{k|t}, \mathbf{u}_k, \hat{\mathbf{w}}_{k|t}, \Delta t) = \mathbf{0}, \quad (7d)$$

where $\mathbf{F}_k = \nabla_{\hat{\mathbf{x}}_{k|t}} \mathbf{f}$, $\mathbf{G}_k = \nabla_{\hat{\mathbf{w}}_{k|t}} \mathbf{f}$, $\mathbf{H}_k = \nabla_{\hat{\mathbf{x}}_{k|t}} \mathbf{h}$, and $\boldsymbol{\lambda}_t^* = \mathbf{0}$ by definition. Differentiating the KKT conditions (7) w.r.t $\boldsymbol{\theta}$ yields the following differential KKT conditions.

$$\begin{aligned} \frac{d \nabla_{\hat{\mathbf{x}}_{t-N|t}} \mathcal{L}}{d \boldsymbol{\theta}} &= \mathbf{L}_{t-N}^{xx} \nabla_{\boldsymbol{\theta}} \hat{\mathbf{x}}_{t-N|t} - \mathbf{P} \nabla_{\boldsymbol{\theta}} \hat{\mathbf{x}}_{t-N} + \mathbf{L}_{t-N}^{x\theta} \\ &+ \mathbf{L}_{t-N}^{xw} \nabla_{\boldsymbol{\theta}} \hat{\mathbf{w}}_{t-N|t} - \mathbf{F}_{t-N}^T \nabla_{\boldsymbol{\theta}} \boldsymbol{\lambda}_{t-N}^* = \mathbf{0}, \end{aligned} \quad (8a)$$

$$\begin{aligned} \frac{d \nabla_{\hat{\mathbf{x}}_{k|t}} \mathcal{L}}{d \boldsymbol{\theta}} &= \mathbf{L}_k^{xx} \nabla_{\boldsymbol{\theta}} \hat{\mathbf{x}}_{k|t} + \mathbf{L}_k^{xw} \nabla_{\boldsymbol{\theta}} \hat{\mathbf{w}}_{k|t} - \mathbf{F}_k^T \nabla_{\boldsymbol{\theta}} \boldsymbol{\lambda}_k^* \\ &+ \nabla_{\boldsymbol{\theta}} \boldsymbol{\lambda}_{k-1}^* + \mathbf{L}_k^{x\theta} = \mathbf{0}, \end{aligned} \quad (8b)$$

$$\begin{aligned} \frac{d \nabla_{\hat{\mathbf{w}}_{k|t}} \mathcal{L}}{d \boldsymbol{\theta}} &= \mathbf{L}_k^{wx} \nabla_{\boldsymbol{\theta}} \hat{\mathbf{x}}_{k|t} + \mathbf{L}_k^{ww} \nabla_{\boldsymbol{\theta}} \hat{\mathbf{w}}_{k|t} \\ &- \mathbf{G}_k^T \nabla_{\boldsymbol{\theta}} \boldsymbol{\lambda}_k^* + \mathbf{L}_k^{w\theta} = \mathbf{0}, \end{aligned} \quad (8c)$$

$$\begin{aligned} \frac{d \nabla_{\boldsymbol{\lambda}_k^*} \mathcal{L}}{d \boldsymbol{\theta}} &= \nabla_{\boldsymbol{\theta}} \hat{\mathbf{x}}_{k+1|t} - \mathbf{F}_k \nabla_{\boldsymbol{\theta}} \hat{\mathbf{x}}_{k|t} - \mathbf{G}_k \nabla_{\boldsymbol{\theta}} \hat{\mathbf{w}}_{k|t} = \mathbf{0}, \end{aligned} \quad (8d)$$

where $\mathbf{L}_k^{xx} = \frac{\partial^2 \mathcal{L}}{\partial \hat{\mathbf{x}}_{k|t}^2}$, $\mathbf{L}_k^{xw} = \frac{\partial^2 \mathcal{L}}{\partial \hat{\mathbf{x}}_{k|t} \partial \hat{\mathbf{w}}_{k|t}}$, $\mathbf{L}_k^{x\theta} = \frac{\partial^2 \mathcal{L}}{\partial \hat{\mathbf{x}}_{k|t} \partial \boldsymbol{\theta}}$, $\mathbf{L}_k^{ww} = \frac{\partial^2 \mathcal{L}}{\partial \hat{\mathbf{w}}_{k|t}^2}$, $\mathbf{L}_k^{wx} = \frac{\partial^2 \mathcal{L}}{\partial \hat{\mathbf{w}}_{k|t} \partial \hat{\mathbf{x}}_{k|t}}$, and $\mathbf{L}_k^{w\theta} = \frac{\partial^2 \mathcal{L}}{\partial \hat{\mathbf{w}}_{k|t} \partial \boldsymbol{\theta}}$.

It has been shown in [15] that (8) can be interpreted as the KKT conditions of an auxiliary linear MHE problem:

$$\begin{aligned} \min_{\mathbf{X}, \mathbf{W}} J_2 &= \frac{1}{2} \text{Tr} \left\| \mathbf{X}_{t-N} - \hat{\mathbf{X}}_{t-N} \right\|_P^2 \\ &+ \text{Tr} \sum_{k=t-N}^t \left(\frac{1}{2} \mathbf{X}_k^T \bar{\mathbf{L}}_k^{xx} \mathbf{X}_k + \mathbf{W}_k^T \mathbf{L}_k^{wx} \mathbf{X}_k \right) \\ &+ \text{Tr} \sum_{k=t-N}^{t-1} \left(\frac{1}{2} \mathbf{W}_k^T \mathbf{L}_k^{ww} \mathbf{W}_k + (\mathbf{L}_k^{w\theta})^T \mathbf{W}_k \right) \\ &+ \text{Tr} \sum_{k=t-N}^t \left((\mathbf{L}_k^{x\theta})^T \mathbf{X}_k \right) \end{aligned} \quad (9a)$$

$$\text{s.t. } \mathbf{X}_{k+1} = \mathbf{F}_k \mathbf{X}_k + \mathbf{G}_k \mathbf{W}_k, \quad (9b)$$

where $\mathbf{X} = \{\mathbf{X}_k\}_{k=t-N}^t$, $\mathbf{W} = \{\mathbf{W}_k\}_{k=t-N}^{t-1}$, $\bar{\mathbf{L}}_k^{xx} = \frac{\partial^2 \bar{\mathcal{L}}}{\partial \hat{\mathbf{x}}_{k|t}^2}$ with $\bar{\mathcal{L}}$ obtained by excluding the arrival cost (See (2a)) from \mathcal{L} , and $\text{Tr}(\cdot)$ is the matrix trace. The optimal solution $\hat{\mathbf{X}}$ to Problem (9) has proved to be exactly the gradient $\nabla_{\boldsymbol{\theta}} \hat{\mathbf{x}}$, denoted as $\hat{\mathbf{X}} = \{\nabla_{\boldsymbol{\theta}} \hat{\mathbf{x}}_{k|t}\}_{k=t-N}^t$. In [15], we proposed an efficient recursive method for computing $\hat{\mathbf{X}}$ using a Kalman filter, which consists of three recursions.

First, a Kalman filter (KF) is solved to obtain the estimates $\{\hat{\mathbf{X}}_{k|k}^{\text{KF}}\}_{k=t-N}^t$: the initial condition is given by

$$\hat{\mathbf{X}}_{t-N|t-N}^{\text{KF}} = (\mathbf{I} + \mathbf{C}_{t-N} \mathbf{S}_{t-N}) \hat{\mathbf{X}}_{t-N} + \mathbf{C}_{t-N} \mathbf{T}_{t-N}. \quad (10)$$

where \mathbf{I} is an identity matrix, \mathbf{C}_{t-N} is defined in (11c) with $\mathbf{P}_{t-N} = \mathbf{P}^{-1}$, \mathbf{S}_{t-N} and \mathbf{T}_{t-N} are given in (12), and $\hat{\mathbf{X}}_{t-N}$ is approximated by $\nabla_{\boldsymbol{\theta}} \hat{\mathbf{x}}_{t-N|t-1}$ obtained at $t-1$. Then, the remaining estimates are generated through the following equations from $k = t-N+1$ to t :

$$\hat{\mathbf{X}}_{k|k-1} = \bar{\mathbf{F}}_{k-1} \hat{\mathbf{X}}_{k-1|k-1}^{\text{KF}} - \mathbf{A}_{k-1}, \quad (11a)$$

$$\mathbf{P}_k = \bar{\mathbf{F}}_{k-1} \mathbf{C}_{k-1} \bar{\mathbf{F}}_{k-1}^T + \mathbf{B}_{k-1}, \quad (11b)$$

$$\mathbf{C}_k = (\mathbf{I} - \mathbf{P}_k \mathbf{S}_k)^{-1} \mathbf{P}_k, \quad (11c)$$

$$\hat{\mathbf{X}}_{k|k}^{\text{KF}} = (\mathbf{I} + \mathbf{C}_k \mathbf{S}_k) \hat{\mathbf{X}}_{k|k-1} + \mathbf{C}_k \mathbf{T}_k. \quad (11d)$$

where \mathbf{A}_k , \mathbf{B}_k , \mathbf{S}_k , \mathbf{T}_k , and $\bar{\mathbf{F}}_k$ are defined below:

$$\mathbf{A}_k = \mathbf{G}_k (\mathbf{L}_k^{ww})^{-1} \mathbf{L}_k^{w\theta},$$

$$\mathbf{B}_k = \mathbf{G}_k (\mathbf{L}_k^{ww})^{-1} \mathbf{G}_k^T,$$

$$\mathbf{S}_k = \mathbf{L}_k^{wx} (\mathbf{L}_k^{ww})^{-1} \mathbf{L}_k^{wx} - \bar{\mathbf{L}}_k^{xx}, \quad \mathbf{S}_t = -\bar{\mathbf{L}}_t^{xx}, \quad (12)$$

$$\mathbf{T}_k = \mathbf{L}_k^{wx} (\mathbf{L}_k^{ww})^{-1} \mathbf{L}_k^{w\theta} - \mathbf{L}_k^{x\theta}, \quad \mathbf{T}_t = -\mathbf{L}_t^{x\theta},$$

$$\bar{\mathbf{F}}_k = \mathbf{F}_k - \mathbf{G}_k (\mathbf{L}_k^{ww})^{-1} \mathbf{L}_k^{wx}.$$

Second, the new dual variables $\boldsymbol{\Lambda}^* = \{\boldsymbol{\Lambda}_k^*\}_{k=t-N}^{t-1}$ are computed using the following equation backward in time from $k = t$ to $t-N+1$, starting with $\boldsymbol{\Lambda}_t^* = \mathbf{0}$:

$$\boldsymbol{\Lambda}_{k-1}^* = (\mathbf{I} + \mathbf{S}_k \mathbf{C}_k) \bar{\mathbf{F}}_k^T \boldsymbol{\Lambda}_k^* + \mathbf{S}_k \hat{\mathbf{X}}_{k|k}^{\text{KF}} + \mathbf{T}_k. \quad (13)$$

Third, the optimal estimates $\hat{\mathbf{X}}$ are obtained using

$$\hat{\mathbf{X}}_{k|t} = \hat{\mathbf{X}}_{k|k}^{\text{KF}} + \mathbf{C}_k \bar{\mathbf{F}}_k^T \Lambda_k^*, \quad (14)$$

iteratively from $k = t - N$ to t .

Note that (11) is not presented in the standard form of a Kalman filter for the purpose of a clearer and more inductive proof, as explained in [15]. The more familiar form can be readily derived. For instance, the standard Kalman gain can be extracted from (11d) using the matrix inversion lemma [25]. The Kalman filter provides analytical gradients in a recursive form, significantly enhancing computational efficiency. The aforementioned recursions are summarized in Algorithm 1.

Algorithm 1: Solving for $\hat{\mathbf{X}}$ using a Kalman filter

Input: $\hat{\mathbf{X}}_{t-N}$ and the matrices in (12);
def *Kalman_Filter_based_Gradient_Solver*:
 1 Set $\hat{\mathbf{X}}_{t-N|t-N}^{\text{KF}}$ using Eq.(10);
 2 **for** $k \leftarrow t - N + 1$ **to** t **by** 1 **do**
 3 Update $\hat{\mathbf{X}}_{k|k}^{\text{KF}}$ using a Kalman filter (11);
 4 **end for**
 5 **for** $k \leftarrow t$ **to** $t - N + 1$ **by** -1 **do**
 6 Update Λ_{k-1}^* using Eq.(13) with $\Lambda_t^* = \mathbf{0}$;
 7 **end for**
 8 **for** $k \leftarrow t - N$ **to** t **by** 1 **do**
 9 Update $\hat{\mathbf{X}}_{k|t}$ using Eq.(14);
 10 **end for**
 11 **return** $\left\{ \hat{\mathbf{X}}_{k|t} \right\}_{k=t-N}^t$
Output: $\nabla_{\theta} \hat{\mathbf{x}} = \hat{\mathbf{X}}$

B. Kalman Filter-based Hessian Solver

Next, we will show that the Hessian of the loss function can also be efficiently computed using a new auxiliary linear MHE. Remarkably, it leverages the same Kalman filter and much of the computation already used to obtain the gradient.

Let $H_p f(x(p), p)$ denote the total second-order derivative of f w.r.t p accounting for possible dependence of x on p , and \otimes the Kronecker product. The Hessian of $L(\hat{\mathbf{x}}(\boldsymbol{\varpi}))$ w.r.t $\boldsymbol{\varpi}$ can be obtained using the chain rule of matrix calculus:

$$\begin{aligned} H_{\boldsymbol{\varpi}} L(\hat{\mathbf{x}}(\boldsymbol{\varpi})) &= (\nabla_{\theta} \hat{\mathbf{x}})^T H_{\hat{\mathbf{x}}} L \nabla_{\theta} \hat{\mathbf{x}} (\nabla_{\boldsymbol{\varpi}} \boldsymbol{\theta})^2 \\ &\quad + (\nabla_{\boldsymbol{\varpi}} \boldsymbol{\theta})^T H_{\theta} \hat{\mathbf{x}} \left[(\nabla_{\hat{\mathbf{x}}} L)^T \otimes \mathbf{I} \right] \nabla_{\boldsymbol{\varpi}} \boldsymbol{\theta} \\ &\quad + [(\nabla_{\hat{\mathbf{x}}} L \nabla_{\theta} \hat{\mathbf{x}}) \otimes \mathbf{I}] H_{\boldsymbol{\varpi}} \boldsymbol{\theta}. \end{aligned} \quad (15)$$

Note that all the first-order derivatives have been obtained in computing the gradient of $L(\hat{\mathbf{x}}(\boldsymbol{\varpi}))$ w.r.t $\boldsymbol{\varpi}$. Computing the second-order derivatives $H_{\hat{\mathbf{x}}} L$ and $H_{\boldsymbol{\varpi}} \boldsymbol{\theta}$ is straightforward, just like their first-order counterparts. The only challenge remains in the computation of $H_{\theta} \hat{\mathbf{x}}$.

Given the implicit dependence of $\hat{\mathbf{x}}$ on $\boldsymbol{\theta}$ and the method for computing $\nabla_{\theta} \hat{\mathbf{x}}$, we are motivated to differentiate the

KKT conditions (7) w.r.t $\boldsymbol{\theta}$ twice. This results in the following second-order differential KKT conditions.

$$\begin{aligned} H_{\theta} \nabla_{\hat{\mathbf{x}}_{t-N|t}} \mathcal{L} &= \dot{\mathbf{L}}_{t-N}^{xx} H_{\theta} \hat{\mathbf{x}}_{t-N|t} - \dot{\mathbf{P}} H_{\theta} \hat{\mathbf{x}}_{t-N} + \dot{\mathbf{L}}_{t-N}^{x\theta} \\ &\quad + \dot{\mathbf{L}}_{t-N}^{xw} H_{\theta} \hat{\mathbf{w}}_{t-N|t} - \dot{\mathbf{F}}_{t-N}^T H_{\theta} \Lambda_{t-N}^* = \mathbf{0}, \end{aligned} \quad (16a)$$

$$\begin{aligned} H_{\theta} \nabla_{\hat{\mathbf{x}}_{k|t}} \mathcal{L} &= \dot{\mathbf{L}}_k^{xx} H_{\theta} \hat{\mathbf{x}}_{k|t} + \dot{\mathbf{L}}_k^{xw} H_{\theta} \hat{\mathbf{w}}_{k|t} - \dot{\mathbf{F}}_k^T H_{\theta} \Lambda_k^* \\ &\quad + H_{\theta} \Lambda_{k-1}^* + \dot{\mathbf{L}}_k^{x\theta} = \mathbf{0}, \end{aligned} \quad (16b)$$

$$\begin{aligned} H_{\theta} \nabla_{\hat{\mathbf{w}}_{k|t}} \mathcal{L} &= \dot{\mathbf{L}}_k^{wx} H_{\theta} \hat{\mathbf{x}}_{k|t} + \dot{\mathbf{L}}_k^{ww} H_{\theta} \hat{\mathbf{w}}_{k|t} \\ &\quad - \dot{\mathbf{G}}_k^T H_{\theta} \Lambda_k^* + \dot{\mathbf{L}}_k^{w\theta} = \mathbf{0}, \end{aligned} \quad (16c)$$

$$\begin{aligned} H_{\theta} \nabla_{\Lambda_k^*} \mathcal{L} &= H_{\theta} \hat{\mathbf{x}}_{k+1|t} - \dot{\mathbf{F}}_k H_{\theta} \hat{\mathbf{x}}_{k|t} - \dot{\mathbf{G}}_k H_{\theta} \hat{\mathbf{w}}_{k|t} \\ &\quad + \dot{\mathbf{L}}_k^{\lambda\theta} = \mathbf{0}, \end{aligned} \quad (16d)$$

where the coefficient matrices are defined below:

$$\begin{aligned} \dot{\mathbf{L}}_k^{xx} &= \mathbf{I} \otimes \mathbf{L}_k^{xx}, \quad \dot{\mathbf{F}}_k = \mathbf{I} \otimes \mathbf{F}_k, \quad \dot{\mathbf{G}}_k = \mathbf{I} \otimes \mathbf{G}_k, \\ \dot{\mathbf{L}}_k^{xw} &= \mathbf{I} \otimes \mathbf{L}_k^{xw}, \quad \dot{\mathbf{L}}_k^{ww} = \mathbf{I} \otimes \mathbf{L}_k^{ww}, \quad \dot{\mathbf{P}} = \mathbf{I} \otimes \mathbf{P}, \\ \dot{\mathbf{L}}_{t-N}^{x\theta} &= (\nabla_{\hat{\mathbf{x}}_{t-N|t}} \bar{\mathbf{f}}_0) \hat{\mathbf{X}}_{t-N|t} + (\nabla_{\Lambda_{t-N}} \bar{\mathbf{f}}_0) \Lambda_{t-N}^* \\ &\quad + (\nabla_{\hat{\mathbf{w}}_{t-N|t}} \bar{\mathbf{f}}_0) \hat{\mathbf{W}}_{t-N|t} + \nabla_{\theta} \bar{\mathbf{f}}_0, \\ \dot{\mathbf{L}}_k^{x\theta} &= (\nabla_{\hat{\mathbf{x}}_{k|t}} \bar{\mathbf{f}}_k) \hat{\mathbf{X}}_{k|t} + (\nabla_{\hat{\mathbf{w}}_{k|t}} \bar{\mathbf{f}}_k) \hat{\mathbf{W}}_{k|t} \\ &\quad + (\nabla_{\Lambda_k^*} \bar{\mathbf{f}}_k) \Lambda_k^* + \nabla_{\theta} \bar{\mathbf{f}}_k, \\ \dot{\mathbf{L}}_k^{w\theta} &= (\nabla_{\hat{\mathbf{x}}_{k|t}} \bar{\mathbf{g}}_k) \hat{\mathbf{X}}_{k|t} + (\nabla_{\hat{\mathbf{w}}_{k|t}} \bar{\mathbf{g}}_k) \hat{\mathbf{W}}_{k|t} \\ &\quad + (\nabla_{\Lambda_k^*} \bar{\mathbf{g}}_k) \Lambda_k^* + \nabla_{\theta} \bar{\mathbf{g}}_k, \\ \dot{\mathbf{L}}_k^{\lambda\theta} &= (\nabla_{\hat{\mathbf{x}}_{k|t}} \bar{\mathbf{h}}_k) \hat{\mathbf{X}}_{k|t} + (\nabla_{\hat{\mathbf{w}}_{k|t}} \bar{\mathbf{h}}_k) \hat{\mathbf{W}}_{k|t}, \end{aligned} \quad (17)$$

with $\bar{\mathbf{f}}_0$, $\bar{\mathbf{f}}_k$, $\bar{\mathbf{g}}_k$, and $\bar{\mathbf{h}}_k$ denoting the left hand sides of (8).

It is interesting to notice that (16) and (8) share exactly the same structure. The only exception lies in (16d) which has an additional term $\dot{\mathbf{L}}_k^{\lambda\theta}$, compared with (8d). As shown in III-A and [15], (8) can represent the KKT conditions of the auxiliary MHE optimization problem (9), which is subject to the linear system (9b) constructed from (8d). Given this observation and concept, we can interpret (16) as the KKT conditions of another auxiliary MHE optimization problem. It is subject to a new linear system constructed from (16d):

$$\dot{\mathbf{X}}_{k+1} = \dot{\mathbf{F}}_k \dot{\mathbf{X}}_k + \dot{\mathbf{G}}_k \dot{\mathbf{W}}_k - \dot{\mathbf{L}}_k^{\lambda\theta}, \quad (18)$$

where $\dot{\mathbf{X}}_k$ and $\dot{\mathbf{W}}_k$ denote $H_{\theta} \hat{\mathbf{x}}_k$ and $H_{\theta} \hat{\mathbf{w}}_k$, respectively. The related cost function can be established directly from (9a) by updating the latter's coefficient matrices, for example, by replacing \mathbf{P} with $\dot{\mathbf{P}}$ defined in (17). Consequently, we can efficiently reuse Algorithm 1 to solve for the MHE Hessian $H_{\theta} \hat{\mathbf{x}}$, which is the optimal solution $\hat{\mathbf{X}}$ to the new auxiliary linear MHE problem. Only the algorithm's inputs need minor modifications as follows:

- Replace $\hat{\mathbf{X}}_{t-N}$ with $\hat{\mathbf{X}}_{t-N}$ (which is approximated by $H_{\theta} \hat{\mathbf{x}}_{t-N|t-1}$ obtained at $t-1$);
- Update the coefficient matrices in (12) using (17), and add the additional term $\dot{\mathbf{L}}_k^{\lambda\theta}$ to \mathbf{A}_k such that the updated \mathbf{A}_k becomes $\dot{\mathbf{A}}_k = \dot{\mathbf{G}}_k \left(\dot{\mathbf{L}}_k^{ww} \right)^{-1} \dot{\mathbf{L}}_k^{w\theta} + \dot{\mathbf{L}}_k^{\lambda\theta}$.

IV. TRUST-REGION LEARNING FRAMEWORK

We aim to train the neural network's parameters $\boldsymbol{\varpi}$ using the trust-region method, which addresses Problem (4) by creating a trust region around the current parameters $\boldsymbol{\varpi}_t$. Within this region, it minimizes a locally quadratic approximation of $L(\hat{\mathbf{x}}(\boldsymbol{\varpi}_t))$ to determine a candidate update $\boldsymbol{\mu}$ for $\boldsymbol{\varpi}_t$. The corresponding optimization problem is as follows:

$$\min_{\boldsymbol{\mu}} \text{TSM}(\boldsymbol{\mu}) = L + \boldsymbol{\mu}^T \nabla_{\boldsymbol{\varpi}_t} L + \frac{1}{2} \boldsymbol{\mu}^T (\mathbf{H}_{\boldsymbol{\varpi}_t} L) \boldsymbol{\mu} \quad (19a)$$

$$\text{s.t. } \|\boldsymbol{\mu}\| \leq \Delta_t. \quad (19b)$$

Given predefined thresholds $0 \leq \gamma_1 \leq \gamma_2 < \gamma_3$, $\kappa_1 \in (0, 1)$, $\kappa_2 > 1$, and the upper bound of the radius $\bar{\Delta}$, the method iteratively explores the trust region by updating its radius $\Delta_t \in \mathbb{R}_+$ with the following law [26]:

$$\Delta_{t+1} = \begin{cases} \kappa_1 \Delta_t & \text{if } \rho_t < \gamma_2 \\ \min(\kappa_2 \Delta_t, \bar{\Delta}) & \text{if } \rho_t > \gamma_3 \& \|\boldsymbol{\mu}_t\| = \Delta_t \\ \Delta_t & \text{otherwise} \end{cases} \quad (20)$$

Here, ρ_t denotes the current ratio between the actual and predicted reductions on the loss function

$$\rho_t = \frac{L(\hat{\mathbf{x}}(\boldsymbol{\varpi}_t)) - L(\hat{\mathbf{x}}(\boldsymbol{\varpi}_t + \boldsymbol{\mu}_t))}{\text{TSM}(\mathbf{0}) - \text{TSM}(\boldsymbol{\mu}_t)}, \quad (21)$$

which is used to decide whether to update $\boldsymbol{\varpi}_t$: if $\rho_t > \gamma_1$, $\boldsymbol{\varpi}_t$ will be updated using $\boldsymbol{\mu}_t$. We summarize the trust-region policy optimization for training NeuroMHE in Algorithm 2.

Algorithm 2: Trust-region NeuroMHE training

Input: The desired states \mathcal{S} and the measurements \mathcal{Y} .

```

1 while  $L_{\text{mean}}$  not converged do
2   for  $t \leftarrow 0$  to  $T$  do
3     Obtain  $\hat{\mathbf{x}}(\boldsymbol{\varpi}_t)$  by solving NeuroMHE  $(\boldsymbol{\varpi}_t)$ 
4     with the most recent measurements  $\mathbf{y} \in \mathcal{Y}$ ;
5     Compute  $L(\hat{\mathbf{x}}(\boldsymbol{\varpi}_t))$  using  $\hat{\mathbf{x}}(\boldsymbol{\varpi}_t)$  and  $\mathbf{s} \in \mathcal{S}$ ;
6     Compute  $\nabla_{\boldsymbol{\varpi}_t} L$  using (5) and Algorithm 1;
7     Compute  $\mathbf{H}_{\boldsymbol{\varpi}_t} L$  using (15) and Algorithm 1
8     with its inputs updated by (17);
9     Obtain  $\boldsymbol{\mu}_t$  by solving TSM Problem (19);
10    Obtain  $\hat{\mathbf{x}}(\boldsymbol{\varpi}_t + \boldsymbol{\mu}_t)$  by solving
11      NeuroMHE  $(\boldsymbol{\varpi}_t + \boldsymbol{\mu}_t)$  with the same  $\mathbf{y}$ ;
12      Compute  $L(\hat{\mathbf{x}}(\boldsymbol{\varpi}_t + \boldsymbol{\mu}_t))$  using  $\hat{\mathbf{x}}(\boldsymbol{\varpi}_t + \boldsymbol{\mu}_t)$ 
13      and the same  $\mathbf{s}$ ;
14      Update  $\rho_t$  using (21);
15      Update  $\Delta_t$  using (20);
16      if  $\rho_t > \gamma_1$  then
17        | Update  $\boldsymbol{\varpi}_{t+1} \leftarrow \boldsymbol{\varpi}_t + \boldsymbol{\mu}_t$ ;
18      else
19        |  $\boldsymbol{\varpi}_{t+1} \leftarrow \boldsymbol{\varpi}_t$ ;
20      end if
21    end for
22    Compute the mean loss  $L_{\text{mean}} = \frac{1}{T} \sum_{t=0}^T L(\hat{\mathbf{x}})$ 
23    for the next episode
24 end while

```

V. SIMULATION RESULTS

We numerically validate the performance of trust-region NeuroMHE in estimating complex aerodynamic disturbances on quadrotors using a real flight dataset from various agile flights [13]. We compare it with the gradient descent counterpart and the state-of-the-art estimator NeuroBEM [13] to showcase the following advantages: 1) highly-efficient training; 2) improved robustness to network initialization; and 3) superior force estimation accuracy.

Consistent with NeuroBEM, we train NeuroMHE from estimation errors. In Algorithm 2, we define the desired states \mathcal{S} using the ground truth disturbance forces \mathbf{F} and torques $\boldsymbol{\tau}$ from the real dataset and the quadrotor model. For NeuroMHE, the measurements \mathcal{Y} are set as the quadrotor's linear \mathbf{v} and angular velocities $\boldsymbol{\omega}$. In contrast, the NeuroBEM's inputs also include the motor speeds, which typically necessitates specialized sensors and autopilot firmware. To address the state estimation problem (2), we augment these velocities with the unmeasurable disturbances to form the augmented state $\mathbf{x} = [\mathbf{v}; \mathbf{F}; \boldsymbol{\omega}; \boldsymbol{\tau}] \in \mathbb{R}^{12}$. Without loss of generality, the dynamics of disturbances are assumed to be driven by the process noises $\mathbf{w}_f \in \mathbb{R}^3$ and $\mathbf{w}_\tau \in \mathbb{R}^3$. The system model for state prediction in MHE is as follows:

$$\dot{\mathbf{v}} = m^{-1}(-mge_3 + \mathbf{F}), \quad \dot{\mathbf{F}} = \mathbf{w}_f, \quad (22a)$$

$$\dot{\boldsymbol{\omega}} = \mathbf{J}^{-1}(-\boldsymbol{\omega}^\times \mathbf{J} \boldsymbol{\omega} + \boldsymbol{\tau}), \quad \dot{\boldsymbol{\tau}} = \mathbf{w}_\tau, \quad (22b)$$

where $g = 9.81 \text{ m/s}^2$, $e_3 = [0; 0; 1]$, $m = 0.772 \text{ kg}$, and $\mathbf{J} = \text{diag}(0.0025, 0.0021, 0.0043) \text{ kgm}^2$ ¹.

The weighting matrices of NeuroMHE have the following dimensions: $\mathbf{P} \in \mathbb{R}^{12 \times 12}$, $\mathbf{R}_k \in \mathbb{R}^{6 \times 6}$, and $\mathbf{Q}_k \in \mathbb{R}^{6 \times 6}$. Instead of training the neural network to generate all \mathbf{R}_k and \mathbf{Q}_k over an MHE horizon, we introduce two forgetting factors $\gamma_{1,2} \in (0, 1)$ to parameterize the time-varying \mathbf{R}_k and \mathbf{Q}_k by $\mathbf{R}_k = \gamma_1^{t-k} \mathbf{R}_t$ and $\mathbf{Q}_k = \gamma_2^{t-1-k} \mathbf{Q}_{t-1}$. We set \mathbf{P} , \mathbf{R}_t , and \mathbf{Q}_{t-1} to be diagonal matrices to further reduce the size of the network. Finally, we parameterize the diagonal elements as $P_{ii} = \varsigma + p_i^2$, $R_{ii} = \varsigma + r_i^2$, and $Q_{ii} = \varsigma + q_i^2$, where $\varsigma > 0$, to guarantee the positive definiteness. The gradient (5) and Hessian (15) are updated accordingly to incorporate the above parameterization. Our neural network has two hidden layers with the Leaky-ReLU activation function. It takes the measurement $\mathbf{y} = [\mathbf{v}; \boldsymbol{\omega}]$ as inputs, has 8 neurons in each hidden layer, and outputs $\boldsymbol{\Theta} = [p_{1:12}, \gamma_1, r_{1:6}, \gamma_2, q_{1:6}] \in \mathbb{R}^{26}$, resulting in a total of 362 network parameters.

For the training data, we select a 0.25-second-long trajectory segment from a Figure-8 flight. One training episode amounts to training NeuroMHE over this 0.25-second-long dataset once. For the test dataset, we adopt the same dataset as in [13] to compare NeuroMHE with NeuroBEM across 13 unseen agile trajectories. We implement our algorithm using CasADi [28] and conduct the simulations in a workstation with an Intel Core i7-11700K processor.

Before showing the estimation performance of trust-region NeuroMHE, we assess its training efficiency by comparing

¹These inertial values are reported at the NeuroBEM's website https://rpg.ifi.uzh.ch/neuro_bem/Readme.html.

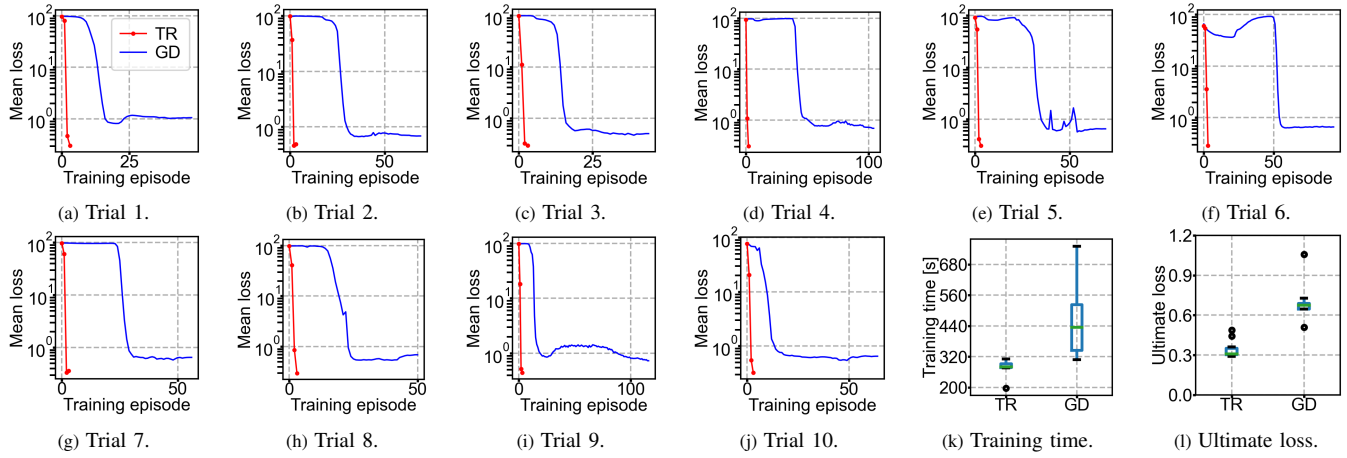


Fig. 2: Comparison of the training performance between the gradient descent (GD) method and the proposed trust-region (TR) method. We randomly initialize the neural network using the Kaiming method [27] in 10 trials. For gradient descent, we set the learning rate to 1×10^{-4} by balancing between training stability and performance. We carefully select the trials of gradient descent such that the untrained mean loss closely matches that of the trust-region method, enabling fair comparisons. The ultimate loss shown in Fig. 2l corresponds to the loss value in the last episode.

the CPU runtime of Algorithm 1 and the overall training time with gradient descent. Table I shows that both methods exhibit roughly linear computational complexity w.r.t the horizon, indicating scalability for large MHE problems. Although computing the MHE Hessian expectedly takes longer than the MHE gradient, the trust-region method significantly reduces the overall training time (under 5 minutes) by up to 63% (See Fig. 2k) while producing better training results (See Fig. 2l). Given the quadrotor’s fast dynamics in agile flights, we set $N = 10$ in the subsequent tests.

TABLE I: Runtime of Algorithm 1 for Different MHE Horizons

Horizon N	10	20	40	60	80
MHE Hessian [ms]	67.5	137.8	253.4	379.3	516.1
MHE Gradient [ms]	1.83	3.74	6.97	12.36	14.93

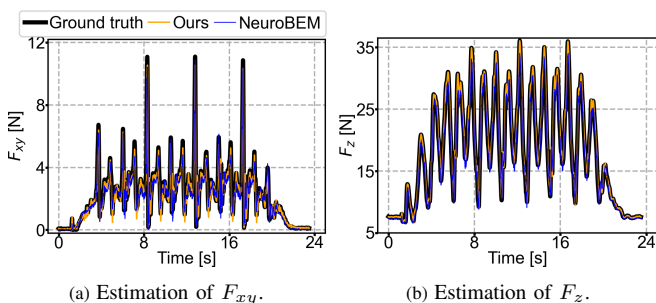


Fig. 3: Comparison of the force estimation performance between NeuroMHE and NeuroBEM on an aggressive Figure-8 flight test dataset as used in [13].

TABLE II: Estimation Errors (RMSEs) Comparisons

Method	F_{xy} [N]	F_z [N]	τ_{xy} [Nm]	τ_z [Nm]	F [N]	τ [Nm]
NeuroBEM	0.51	1.08	0.03	0.01	1.20	0.03
Ours	0.32	0.31	0.02	0.01	0.45	0.02

Fig. 3 compares the force estimation performance between trust-region NeuroMHE and NeuroBEM using an unseen

agile flight dataset. Our method demonstrates high accuracy, even in the challenging force spikes, where NeuroBEM exhibits substantial performance degradation. Table II provides the related quantitative comparisons using the Root-Mean-Square errors (RMSEs). We outperform NeuroBEM significantly in the planar and vertical force estimations with the RMSE reductions of 37.3% and 71.3%, respectively. Further comparisons on the entire NeuroBEM test dataset² show that we substantially improve the overall force estimation performance across most trajectories by up to 68.1%. Note that such a superior generalizability is achieved by training a lightweight network with 362 parameters using only 0.25-second-long data. In contrast, NeuroBEM requires 3150-second-long flight data to train a high-capacity neural network with 25k parameters.

VI. CONCLUSIONS

This paper proposed a trust-region policy optimization method for training NeuroMHE. Our critical insight is that most of the computation initially used to obtain the MHE gradient, especially the Kalman filter, can be efficiently reused for calculating the MHE Hessian in a recursive form. Through extensive simulations using real flight data, we have shown that our method provides highly-efficient training, accurate estimation with fast online adaptation to various challenging scenarios, and improved robustness to network initialization. Our future work includes theoretical analysis of the stability of trust-region NeuroMHE, and simultaneous learning of optimal estimator and controller with second-order optimization techniques.

REFERENCES

[1] M. L. Corradini and G. Orlando, “Robust tracking control of mobile robots in the presence of uncertainties in the dynamical model,” *Journal of robotic systems*, vol. 18, no. 6, pp. 317–323, 2001.

²The results of a comprehensive comparison on entire 13 unseen agile trajectories can be found at <https://github.com/BinghengNUS/TR-NeuroMHE>.

[2] C. Powers, D. Mellinger, A. Kushleyev, B. Kothmann, and V. Kumar, “Influence of aerodynamics and proximity effects in quadrotor flight,” in *Experimental Robotics: The 13th International Symposium on Experimental Robotics*. Springer, 2013, pp. 289–302.

[3] E. Hashemi, M. Pirani, A. Khajepour, B. Fidan, A. Kasaiezadeh, S.-K. Chen, and B. Litkouhi, “Integrated estimation structure for the tire friction forces in ground vehicles,” in *2016 IEEE International Conference on Advanced Intelligent Mechatronics (AIM)*. IEEE, 2016, pp. 1657–1662.

[4] Z. Chu, F. Wang, T. Lei, and C. Luo, “Path planning based on deep reinforcement learning for autonomous underwater vehicles under ocean current disturbance,” *IEEE Transactions on Intelligent Vehicles*, vol. 8, no. 1, pp. 108–120, 2022.

[5] P. Coelho and U. Nunes, “Path-following control of mobile robots in presence of uncertainties,” *IEEE Transactions on Robotics*, vol. 21, no. 2, pp. 252–261, 2005.

[6] B. S. Park, S. J. Yoo, J. B. Park, and Y. H. Choi, “Adaptive neural sliding mode control of nonholonomic wheeled mobile robots with model uncertainty,” *IEEE Transactions on Control Systems Technology*, vol. 17, no. 1, pp. 207–214, 2008.

[7] B. Yüksel, C. Secchi, H. H. Bülthoff, and A. Franchi, “A nonlinear force observer for quadrotors and application to physical interactive tasks,” in *2014 IEEE/ASME international conference on advanced intelligent mechatronics*. IEEE, 2014, pp. 433–440.

[8] T. Tomić and S. Haddadin, “A unified framework for external wrench estimation, interaction control and collision reflexes for flying robots,” in *2014 IEEE/RSJ international conference on intelligent robots and systems*. IEEE, 2014, pp. 4197–4204.

[9] J. Huang, S. Ri, T. Fukuda, and Y. Wang, “A disturbance observer based sliding mode control for a class of underactuated robotic system with mismatched uncertainties,” *IEEE Transactions on Automatic Control*, vol. 64, no. 6, pp. 2480–2487, 2018.

[10] D. Hentzen, T. Stastny, R. Siegwart, and R. Brockers, “Disturbance estimation and rejection for high-precision multirotor position control,” in *2019 IEEE/RSJ International Conference on Intelligent Robots and Systems (IROS)*. IEEE, 2019, pp. 2797–2804.

[11] C. D. McKinnon and A. P. Schoellig, “Estimating and reacting to forces and torques resulting from common aerodynamic disturbances acting on quadrotors,” *Robotics and Autonomous Systems*, vol. 123, p. 103314, 2020.

[12] X. Liu, C. Yang, Z. Chen, M. Wang, and C.-Y. Su, “Neuro-adaptive observer based control of flexible joint robot,” *Neurocomputing*, vol. 275, pp. 73–82, 2018.

[13] L. Bauersfeld, E. Kaufmann, P. Foehn, S. Sun, and D. Scaramuzza, “Neurobem: Hybrid aerodynamic quadrotor model,” *Proceedings of Robotics: Science and Systems XVII*, p. 42, 2021.

[14] G. Shi, W. Hönig, X. Shi, Y. Yue, and S.-J. Chung, “Neural-swarm2: Planning and control of heterogeneous multirotor swarms using learned interactions,” *IEEE Transactions on Robotics*, vol. 38, no. 2, pp. 1063–1079, 2021.

[15] B. Wang, Z. Ma, S. Lai, and L. Zhao, “Neural moving horizon estimation for robust flight control,” *arXiv preprint arXiv:2206.10397*, 2022.

[16] T. Kraus, H. J. Ferreau, E. Kayacan, H. Ramon, J. De Baerdemaeker, M. Diehl, and W. Saeys, “Moving horizon estimation and nonlinear model predictive control for autonomous agricultural vehicles,” *Computers and electronics in agriculture*, vol. 98, pp. 25–33, 2013.

[17] B. Wang, Z. Ma, S. Lai, L. Zhao, and T. H. Lee, “Differentiable moving horizon estimation for robust flight control,” in *2021 60th IEEE Conference on Decision and Control (CDC)*. IEEE, 2021, pp. 3563–3568.

[18] A. Papadimitriou, H. Jafari, S. S. Mansouri, and G. Nikolakopoulos, “External force estimation and disturbance rejection for micro aerial vehicles,” *Expert Systems with Applications*, vol. 200, p. 116883, 2022.

[19] D. G. Robertson, J. H. Lee, and J. B. Rawlings, “A moving horizon-based approach for least-squares estimation,” *AICHE Journal*, vol. 42, no. 8, pp. 2209–2224, 1996.

[20] H. N. Esfahani, A. B. Kordabadi, and S. Gros, “Reinforcement learning based on mpc/mhe for unmodeled and partially observable dynamics,” in *2021 American Control Conference (ACC)*. IEEE, 2021, pp. 2121–2126.

[21] S. Muntwiler, K. P. Wabersich, and M. N. Zeilinger, “Learning-based moving horizon estimation through differentiable convex optimization layers,” in *Learning for Dynamics and Control Conference*. PMLR, 2022, pp. 153–165.

[22] J. Schulman, S. Levine, P. Abbeel, M. Jordan, and P. Moritz, “Trust region policy optimization,” in *International conference on machine learning*. PMLR, 2015, pp. 1889–1897.

[23] K. Cao and L. Xie, “Trust-region inverse reinforcement learning,” *IEEE Transactions on Automatic Control*, 2023.

[24] A. Alessandri, M. Baglietto, G. Battistelli, and V. Zavala, “Advances in moving horizon estimation for nonlinear systems,” in *49th IEEE Conference on Decision and Control (CDC)*. IEEE, 2010, pp. 5681–5688.

[25] H. Cox, “Estimation of state variables for noisy dynamic systems,” Ph.D. dissertation, Massachusetts Institute of Technology, 1963.

[26] J. Nocedal and S. J. Wright, *Numerical optimization*. Springer, 1999.

[27] K. He, X. Zhang, S. Ren, and J. Sun, “Delving deep into rectifiers: Surpassing human-level performance on imagenet classification,” in *Proceedings of the IEEE international conference on computer vision*, 2015, pp. 1026–1034.

[28] J. A. Andersson, J. Gillis, G. Horn, J. B. Rawlings, and M. Diehl, “Casadi: a software framework for nonlinear optimization and optimal control,” *Mathematical Programming Computation*, vol. 11, no. 1, pp. 1–36, 2019.